A Planar Switchable 3-D-Coverage Phased Array Antenna and Its User Effects for 28-GHz Mobile Terminal Applications

Zhang, Shuai; Chen, Xiaoming; Syrytsin, Igor A.; Pedersen, Gert F.

Published in:
I E E E Transactions on Antennas and Propagation

DOI (link to publication from Publisher):
10.1109/TAP.2017.2681463

Publication date:
2017

Document Version
Accepted author manuscript, peer reviewed version

This article has been accepted for publication in a future issue of this journal, but has not been fully edited. Content may change prior to final publication. Citation information: DOI 10.1109/TAP.2017.2681463, IEEE Transactions on Antennas and Propagation

A Planar Switchable 3D-Coverage Phased Array Antenna and Its User Effects for 28 GHz Mobile Terminal Applications

Shuai Zhang, Xiaoming Chen, Igor Syrytsin, and Gert Frølund Pedersen

***Abstract*—This paper introduces a planar switchable 3D-coverage phased array for 28 GHz mobile terminal applications. In order to realize 3D-coverage beam scan with a simple planar array, chassis surface waves are efficiently excited and controlled by three identical slot subarrays. Three subarrays switch their beams to three distinct regions. Each subarray works as a phased array to steer the beam within each region. Large coverage efficiency is achieved (e.g., 80% of the space sphere has the realized gain of over 8 dBi). The proposed antenna covers a bandwidth of over 2 GHz in the band of 28 GHz. User effects on the switchable array are also studied in both data mode and talk mode (voice) at 28 GHz. In talk mode, good directivity and beam switching can be realized by placing the switchable array at the top of the chassis (close to the index finger). And the user shadowing can be significantly reduced by placing it at the bottom of the chassis (close to the palm). In data mode, the switchable array, mounted at the top, achieves less body loss and larger coverage than at the bottom. The proposed antenna is fabricated and measured. The array at the top in talk mode is measured with a real human. The measurements align well with simulations.**

***Index Terms*—Mobile antenna, planar antenna, phased array, 3D coverage, user effect, 5G application.**

I. Introduction

TRANSMITTING and receiving multi-media data in a higher speed is urgently demanded. As a key technology in the fifth generation (5G) communication systems, millimeter-wave (mm-wave) and centimeter-wave (cm-wave) technology promises Gigabit-per-second data rate [1]-[3]. In mm-/cm-wave bands (e.g., 28 GHz), free-space path loss is much larger than that in conventional cellular bands below 6 GHz [4]-[5], if we assume antenna gain is fixed (and then antenna area reduces with the operating frequency increasing). If phased arrays can be applied in mm-/cm-wave bands with the antenna area the same as that in conventional cellular bands, higher antenna gain can be utilized to compensate the large path loss. Phased arrays with high gain have to be applied at both base stations and mobile handsets [2]. Since high gain leads to narrow radiation beam width, phased arrays must also offer large beam steering range to allow the gain to be used in optimal transmitting-receiving angle. For the base station antenna, there is ample room for complex phased array designs with the high performance of beam scans [6]-[7]. However, in mobile handsets, it is much more challenging to implement mm-/cm-wave phased arrays due to the limited space for antenna designs, user mobility, and user tissue effects.

Recently, some studies have been carried out to investigate phased array antennas in mobile terminals [8]-[12]. In [8], a parameter of coverage efficiency (η_c) has been defined as:

$$\eta_c = \frac{Coverage\ Solid\ Angle}{Maximum\ Solid\ Angle}\Big|_{realized\ gain} \quad (1)$$

where the coverage solid angle is calculated by the total scan pattern higher than a certain realized gain; the maximum solid angle is 4π steradians if the whole sphere is chosen. The coverage efficiency of two types of phased arrays for mobile handsets has been calculated and compared in [8] as well. In [9], a mobile terminal phased array at 3.5 GHz has been introduced by utilizing the slots formed by the metal frame and the ground plane of a mobile handset. The coverage efficiency in the user cases has also been evaluated in [9]. A practical design of 28 GHz phased array has been studied in [10]. In order to further improve the coverage efficiency, a switchable 3D-coverage phased array has been proposed in [11]. However, the antenna in [11] is a 3D design, which is not easy for fabrication and implementation. The suppression of chassis surface waves of handset antennas at 15 GHz has been studied in [12], where the directivity of the antenna has been improved. Furthermore, user effects on mobile terminal antennas have been well studied in conventional cellular bands, e.g., [13]-[15]. However, at 28 GHz literature about user effects are very limited.

In this paper, a planar switchable 3D-coverage phased array antenna is proposed for 28 GHz mobile terminal applications. Instead of suppressing chassis surface waves in [12], the chassis surface waves are efficiently excited and controlled by three identical slot subarrays, so that three switchable beams pointing at three different regions are realized. 3D coverage is achieved by combining the switchable beams of three slot subarrays and the scan beams of each subarray. The proposed

This work was supported by the InnovationsFonden project of RANGE.

Shuai Zhang, Igor Syrytsin and Gert Frølund Pedersen are with the Antennas, Propagation and Radio Networking section at the Department of Electronic Systems, Aalborg University, Denmark (email: sz@es.aau.dk, igs@es.aau.dk, gfp@es.aau.dk).

Xiaoming Chen is with School of Electronic and Information Engineering, Xi'an Jiaotong University, Xi'an 710049, China (email: xiaoming.chen@mail.xjtu.edu.cn).

This article has been accepted for publication in a future issue of this journal, but has not been fully edited. Content may change prior to final publication. Citation information: DOI 10.1109/TAP.2017.2681463, IEEE Transactions on Antennas and Propagation

antenna covers the bandwidth of over 2 GHz at the central frequency of 28 GHz with a large coverage efficiency. Compared to the previous literature, the switchable slot antenna design and the method of utilizing surface waves to enlarge the coverage in this paper are novel. The user effects on the proposed switchable phased array are also studied in this paper. In [16], the variations of user effects on an endfire mobile terminal antenna from 12 different users have been analyzed at 28 GHz. This paper mainly investigates the user effects on the beam switchable property and different radiation patterns of a switchable phased array for a mobile terminal at 28 GHz, which is novel as well. The designed antenna is fabricated and measured to verify the simulations. The measurement of the array at the top in talk mode is also carried out with a real human.

II. Operating Principles

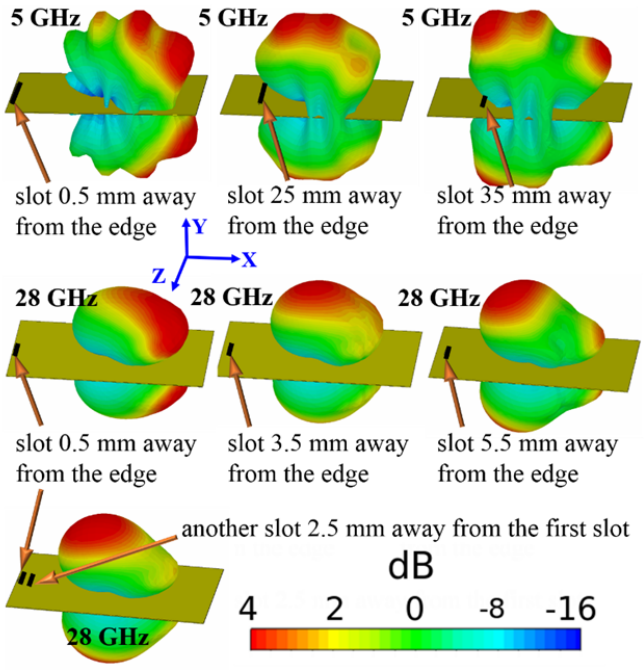

Fig. 1. Gain patterns of one slot antenna with different distances to the mobile chassis short edge at 5 GHz and 28 GHz.

In conventional cellular bands, the radiation patterns of an antenna are highly affected by characteristic modes on a mobile chassis [17]-[19]. In cm-/mm-wave bands (e.g., 28 GHz), the wavelength of the operating frequency is much smaller than the mobile chassis dimension. The antenna radiation patterns are mainly impacted by surface waves on the chassis instead of characteristic modes. One type of surface waves is supported on the interface between two homogeneous media with different dielectric constants (Sommerfeld-Zenneck surface wave). On the interface between a metal plane and free space, surface waves can occur: These surface waves are called surface plasmons at optical frequencies. And at cm-/mm-wave frequencies, these surface waves are often described as surface currents since the surface waves and surface currents have similar skin depth at these frequencies [20]. Another type of surface waves may occur if a dielectric substrate (layer) is placed on the surface of a metal plane. This type of surface waves is trapped within the dielectric substrate layer (trapped surface wave). Depending on the dielectric constant and thickness, the strength of the trapped surface waves at cm-/mm-wave frequencies varies. Since the effects of these two types of surface waves on the radiation patterns of cm-/mm-wave antennas are similar, the following analyses are applied for both types of surface waves. The effectiveness of surface wave excitation depends on the polarization of antennas. In general, the antenna polarization perpendicular to material surface can more efficiently excite surface waves than the antenna polarization parallel to material surface [21]. Slot antennas excite stronger surface waves on a mobile chassis than patch antennas (e.g., used in [11]), planar inverted-f antennas (PIFA) and planar monopole antennas. The reason is that the slot antennas are phi polarized (see the coordinate system in Fig. 1), which provides strong y-axis polarization components (or perpendicular polarization components) on both sides of the slot antenna. However, the polarization of patch antennas, PIFA and planar monopole antennas is mainly parallel to the xz plane. Please note if we make the polarization of patch antennas, PIFA and monopole antennas perpendicular to the ground plane, strong surface waves can also be excited but the antenna structures will not be planar anymore. In this paper, we use slot antennas for strong surface wave excitation while keeping the planar structure.

Fig. 1 shows the radiation patterns of one slot antenna with different distances to the mobile chassis short edge at 5 GHz and 28 GHz. No dielectric substrate is added to the surface of the metal ground plane in Fig. 1, so the trapped surface waves are not available here. If a dielectric substrate is attached on one side of the metal plane, the radiation patterns at two sides of the ground plane will be a little asymmetrical. It can be solved by using a thin and low permittivity dielectric substrate or by placing another substrate on the other side of the ground plane. In Fig. 1, the beam steering can be clearly observed at both frequencies. Please note: due to the strong chassis mode impacts on antenna radiation patterns at 5 GHz, there are more side lobes at 5 GHz than at 28 GHz. The reason for the beam steering property mentioned above is that: the chassis surface waves from one side of the slot antenna are reflected back by the chassis edge and superposed on the surface waves from the other side of the slot antenna. Depending on the distance between the slot and the chassis edge, the main beam is able to scan to different directions in the xy plane (see Fig. 1) without changing the slot antenna dimensions. Apparently, this superposition is also related to the wavelength of operating frequencies. Due to the small wavelength at 28 GHz the slot antenna only needs to move from 0.5 mm to 5.5 mm away from the edge to realize the beam scan, while at 5 GHz the slot-edge distance has to change from 0.5 mm to 35 mm. Furthermore, in Fig. 1 if another slot 2.5 mm away from the first slot at 28 GHz is added, the main beam of the first slot can also change significantly, due to the superposition of the reflected surface waves from another slot antenna. Therefore, at 28 GHz the slot antenna can change the main beam direction with much smaller

This article has been accepted for publication in a future issue of this journal, but has not been fully edited. Content may change prior to final publication. Citation information: DOI 10.1109/TAP.2017.2681463, IEEE Transactions on Antennas and Propagation

side lobes and mobile chassis clearance than at conventional cellular frequencies (e.g., 5 GHz).

The main beam direction of a slot antenna on a mobile chassis is mainly determined by: 1. the distance between the slot antenna and the chassis edge; 2. the distance between the operating slot antenna and the neighbor slot antenna in the x-axis direction (see Fig. 1).

III. Planar 3D-Coverage Phased Array Antenna for 5G Mobile Terminal Applications

A. Antenna Configurations

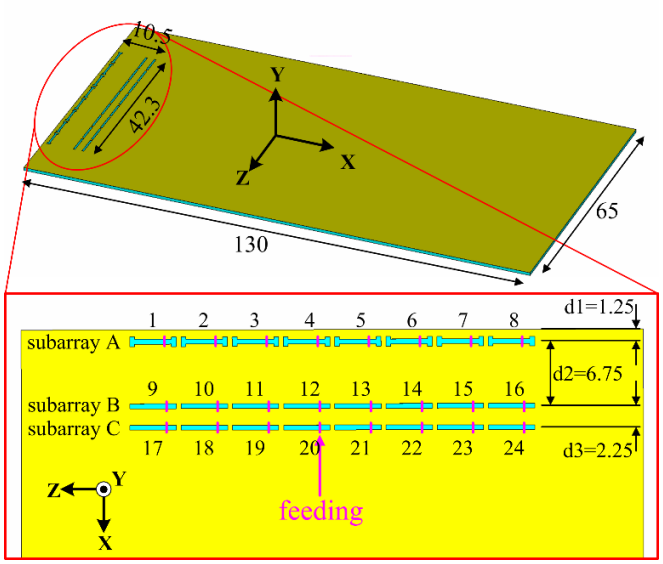

Fig. 2. Antenna configurations on the printed circuit board. (Unit: mm)

By applying the principles in Section II, a planar 3D-coverage phased array antenna is proposed and shown in Fig. 2. The antenna is printed on the Nelco N9000 PCB substrate with a relative permittivity of 2.2, and a loss tangent of 0.0009. The substrate has the size of 65mm ×130mm and the thickness of 0.764 mm. A copper layer is available on only one side of the substrate and some slots are etched on the copper. The designed antenna consists of three slot subarray antennas. Each subarray has 8 slot elements with the length of 4.85 mm and the width of 0.5 mm. In subarray A (see Fig. 2), the two ends of each slot are slightly wider to adjust the operating frequency. The center-to-center and edge-to-edge distances of the neighboring slot elements in each subarray are 5.35 mm and 0.5 mm, respectively. To facilitate simulations in CST, each slot element is fed with a discrete port. The feeding points are 1.5 mm, 1.2 mm and 1.2 mm away from the slot element edges in subarray A, subarray B and subarray C, respectively. In Section III-D, the impacts of feeding array elements with practical coaxial cables will be analyzed. The distances between the subarrays and the chassis short edge are determined by d1, d2 and d3 in Fig. 2. The d1, d2 and d3 have been adjusted according to the principles described in Section II so that the main beam of each subarray covers different regions in the phi direction (see Fig. 2). In the applications, when one subarray is operating the other two subarrays will be terminated with 50-ohm loads. The main beam of the whole array is switched among the three subarrays in the phi direction and is scanned with phase shifts in each subarray in the theta direction (see Fig. 2). In this way, a 3D-coverage property is realized by a simple planar switchable phased array antenna.

B. Antenna Performance

Within each subarray, the reflection coefficients of the subarray elements are very similar. The reflection coefficients of element 4 (in subarray A), element 12 (in subarray B) and element 20 (in subarray C) (see Fig. 2) are shown in Fig. 3. Each subarray covers the impedance bandwidth of over 2 GHz at the central frequency of 28 GHz, which is sufficient for 5G mobile terminal applications. The isolation between the neighboring elements in each subarray is higher than 12.75 dB. In Fig. 3, only $S_{4,12}$ and $S_{12,20}$ are provided, which are lower than -12.3 dB and -9.4 dB, respectively. In fact, the mutual coupling of all the elements between subarray A and subarray B is lower than -12.3 dB, while between subarray B and subarray C is lower than -9.4 dB.

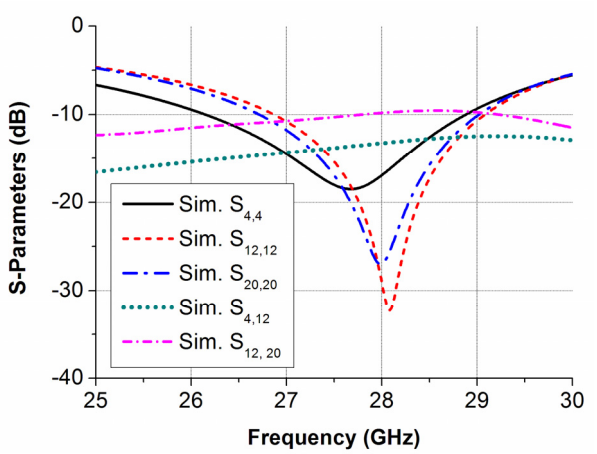

Fig. 3. S-parameters of the proposed antenna with discrete ports for the element 4 in subarray A, element 12 in subarray B and element 20 in subarray C (see Fig. 2).

The radiation gain patterns of the three subarrays are shown in Fig. 4 and Fig. 5. The radiation pattern of each subarray in Fig. 4 is obtained with all the elements in this subarray in phase. The main beams of subarray A, subarray B and subarray C point at phi directions of phi= ±73 degree, phi= ±128 degree and phi= ±20 degree, respectively. By utilizing a switch for all the three subarrays, the 3 dB beam width of the switchable array can cover the phi angles from 6.7 to 152 degree (as well as -16 to -155 degree), as illustrated by arrows in Fig. 4. Since the relative permittivity of the substrate is low (2.2) and the substrate is thin (0.764 mm), the radiation patterns in -y and +y directions in Fig. 4 are nearly symmetric. In order to scan the main beam in the theta direction as well, phase shifts are applied to each subarray. The radiation patterns of three subarrays with different scan angles in theta are shown in Fig. 5. The main beams of subarray A, subarray B and subarray C are steered in the phi planes of 73 degree, 120 degree and 20 degree, respectively. Acceptable realized gain has been obtained for

This article has been accepted for publication in a future issue of this journal, but has not been fully edited. Content may change prior to final publication. Citation information: DOI 10.1109/TAP.2017.2681463, IEEE Transactions on Antennas and Propagation

different scan angles. In addition, the mutual coupling between subarray B and subarray C is lower than -9.4 dB. Mutual coupling between two subarrays may increase envelope correlation coefficient between two switchable radiation patterns and reduce the total efficiency. In this design, the envelope correlation coefficients between the radiation patterns of two subarrays [22] are always lower than 0.07. The total efficiency of the array elements in Subarray A, Subarray B, and Subarray C are around 74.3%, 68%, and 72.2%, respectively. These performance is enough for the application of a switchable phased array for mobile terminals at 28 GHz (and also enough for MIMO applications).

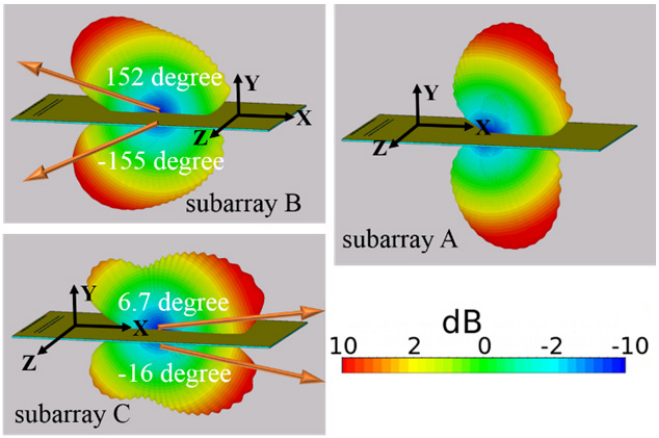

Fig. 4. Radiation gain pattern of each subarray with all elements in phase (steering the main beam in the phi direction).

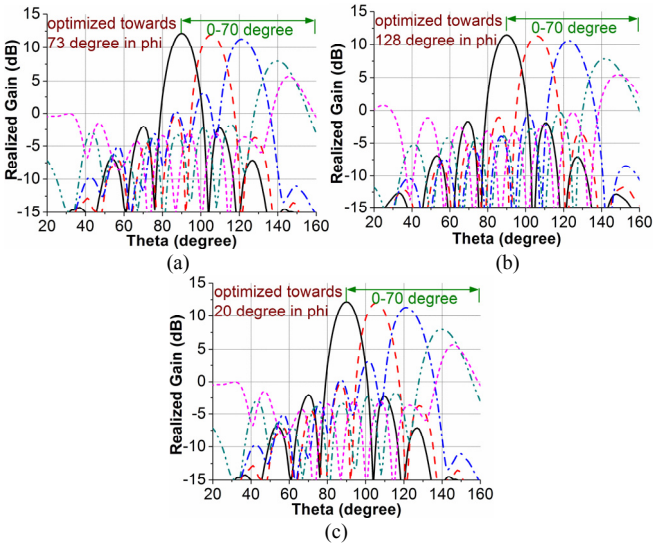

Fig. 5. Radiation gain patterns within the scan angle of 70 degree (steering the main beam in the theta direction): (a) subarray A in the plane of phi=73 degree, (b) subarray B in the plane of phi=128 degree, and (c) subarray C in the plane of phi=20 degree.

The coverage efficiency is used to describe the percentage of the solid angles in the whole sphere with the realized gain higher than a certain value. The coverage efficiency is calculated as follows: each possible beam in each subarray is combined, and then it is calculated how big portion of the maximum solid angle can be covered with the desired gain level. To quantitatively evaluate the realized gain of the scanned beam in the whole sphere, the coverage efficiency is calculated for the proposed switchable phased array and for each individual phased subarray, which is shown in Fig. 6. With the switchable phased array, larger coverage efficiency can be achieved than utilizing only one of the three subarrays: For example, with the realized gain over 8 dBi, the coverage efficiency with the switchable array can be increased by 30%-60% than only applying one subarray (and also by over 40% than applying the optimal array in [8]).

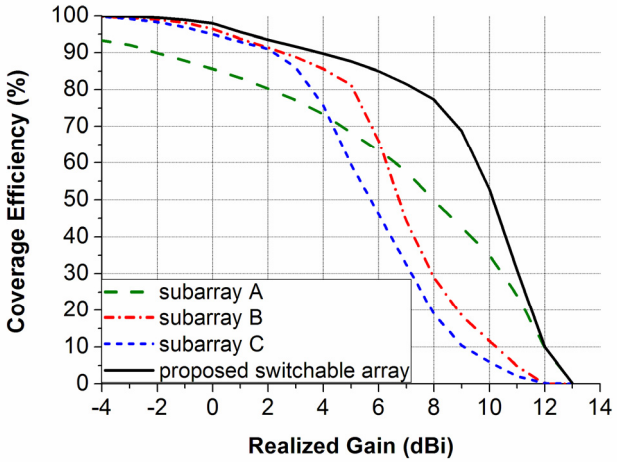

Fig. 6. Coverage efficiency comparison between the proposed switchable phased array antenna and each individual phased subarray.

In addition, the proposed switchable array can also be utilized to significantly shorten the beamforming training period using the hieratical beamforming training scheme [23]. Specifically, for initial beamforming training, instead of scanning every possible angle with beamforming signal (which is time-consuming), we switch over three subarrays sequentially, and select the region with the strongest signal. Then, scan the chosen region with beamforming training signal. In this way, the beamforming training stage can be much shorter.

C. User Effects

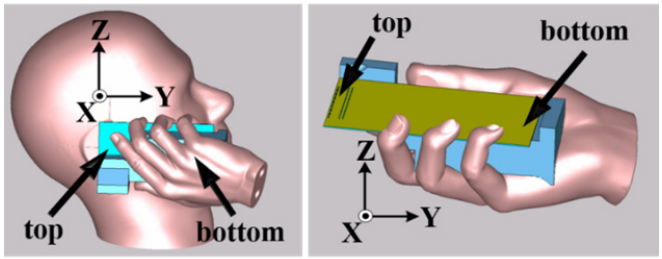

(a) (b)

Fig. 7. User effect simulation setups: (a) talk mode, and (b) data mode.

The user effects on the proposed switchable array are simulated and studied in talk mode and data mode at 28 GHz. Fig. 7 shows the simulation setups, where the “top” and “bottom” means three subarrays are placed at the chassis end close to the index figure and close to the palm, respectively. The electrical parameters for the hand and the head are set as

This article has been accepted for publication in a future issue of this journal, but has not been fully edited. Content may change prior to final publication. Citation information: DOI 10.1109/TAP.2017.2681463, IEEE Transactions on Antennas and Propagation

skin. The permittivity of skin at 28 GHz is set to be: 16.4+16.4j in the simulations. The parameters of different tissues (including skin) up to 100 GHz can be found in [24]. As there is no defined standard for user effect measurements at 28 GHz yet, the mobile terminal is placed according to the CTIA standard for conventional cellular bands [25] in both talk and data modes. At 28 GHz the user's head and hand are electrically large objects and simulating all the elements in each subarray is very time-consuming. To facilitate the simulations, only element 4 in subarray A, element 12 in subarray B and element 20 in subarray C are simulated. When one element is excited, all the other elements shown in Fig. 2 are terminated with 50-ohm loads. The embedded radiation patterns of element 4, element 12 and element 20 can be considered as the mean values for the other elements in subarray A, subarray B and subarray C under user effects, respectively. The body loss is here calculated by subtracting the total efficiency including the user from the total efficiency in free space, where the return loss and mutual coupling between elements are included. In the subarray A (top) of talk mode, the reflection coefficient of the antenna is detuned from -17 dB to -10 dB at 28 GHz. The reflection coefficients of the antennas in the other user cases are always below -15 dB. The antenna detuning due to the hand and the head has very limited effect on the total efficiency.

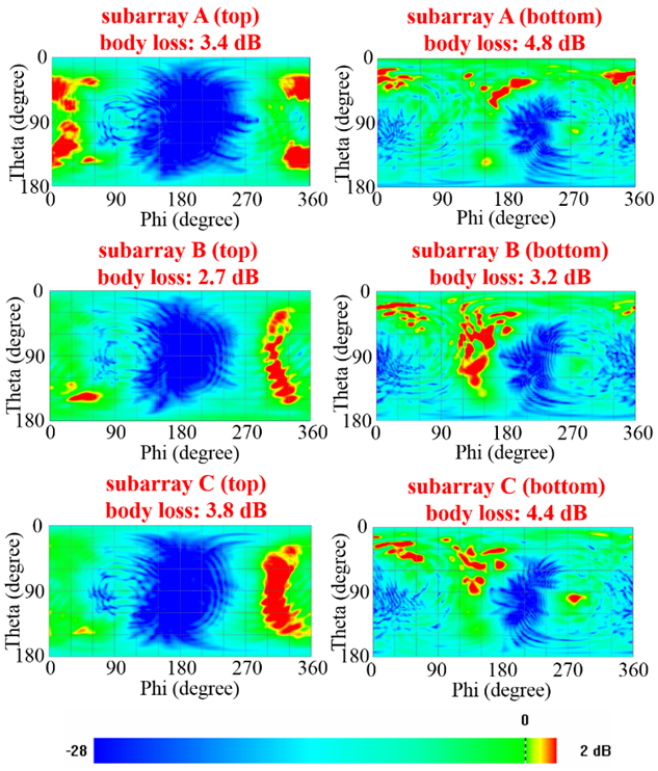

Fig. 8. Gain patterns for each subarray at the top and bottom in the talk mode.

The simulated results in talk mode are shown in Fig. 8. The switchable array at the top gives 0.5-1.4 dB lower body loss, larger antenna directivity and better beam switching than that at the bottom. However, the bottom placement can significantly reduce the shadowing areas of the user's head. The gain in the shadow of the user's head is normally lower than -30 dBi. In most cases, the gain in the shadow can be enlarged by over 15 dB, by moving the switchable array from the top to the bottom. The gain improvement in the user shadow is very meaningful in practical applications. The shadow from fixed objects (e.g., buildings) can be reduced by adding more cell base stations in advance. However, due to the mobility of users, the shadow from user heads occurs and moves randomly, which is difficult to predict and put more base stations in advance to combat. In addition, it is also noticed that in the bottom placement beam switching does not work well, where radiation patterns from different subarrays are very similar.

Gain patterns for the top and bottom placements in data mode are provided in Fig. 9, where the beam switching can be observed clearly. For the top placement, the body loss is 1.2-2 dB lower and the shadowing area is much smaller than that in the bottom location. Therefore, in data mode, the switchable array should be placed at the top. In addition, please note that in the subarray C (top) and subarray A (bottom) of Fig. 9, the main beam points at the user's body. In fact, this property is very useful for the body shadowing reduction.

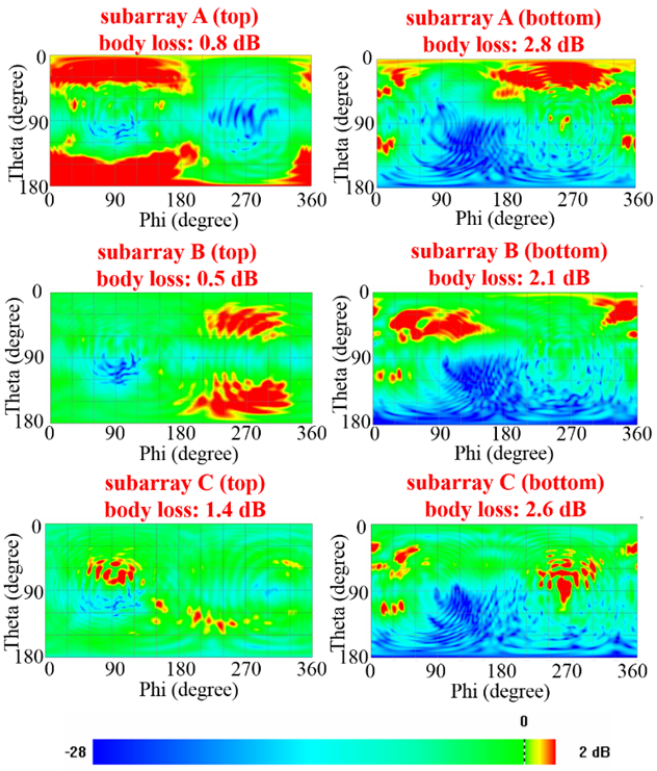

Fig. 9. Gain patterns with top and bottom array locations in the data mode.

Based on the studies above, in practical applications, the switchable array with three subarrays should be placed at the top, where the beam switching, body loss and realized gain are always better than at the bottom. An additional "diversity" linear array can be placed at the bottom to significantly reduce the shadowing in talk mode. In addition, in Fig. 8 different subarrays at the bottom lead to similar radiation patterns in talk mode. Thus, the radiation patterns of the "diversity" linear array at the bottom are not very important.

This article has been accepted for publication in a future issue of this journal, but has not been fully edited. Content may change prior to final publication. Citation information: DOI 10.1109/TAP.2017.2681463, IEEE Transactions on Antennas and Propagation

D. *Impacts of Antenna Feeding Cables for Implementations*

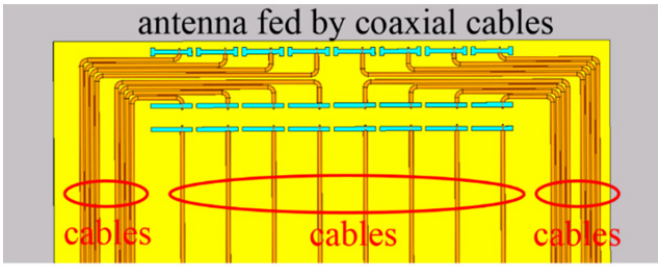

(a)

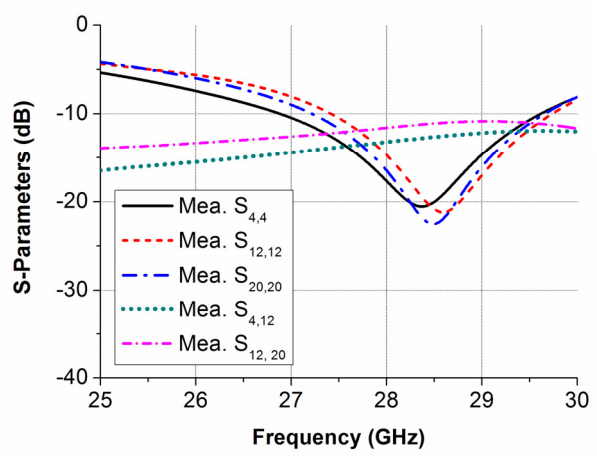

(b)

Fig. 10. Impacts of antenna feeding cables: (a) the proposed phased array antenna with feeding cables, and (b) S-parameters with feeding cables for the element 4 in subarray A, element 12 in subarray B and element 20 in subarray C (see Fig. 2).

In practical applications, the switchable phased array can be fed with several 50 ohm thin coaxial cables as shown in Fig. 10 (a). The diameter of the coaxial cable is about 0.51 mm, which is commercially available. The feeding points of the coaxial cables are the same as the discrete ports in Fig. 2. In order to compare with the results using discrete port feeding, the S-parameters of the element 4, element 12 and element 20 (see Fig. 2) are simulated with thin coaxial cable, as shown in Fig. 10 (b). The S-parameters in Fig. 10 are similar to those in Fig. 3, which means the coaxial cable feeding can be used in practical implementations. Furthermore, to limit page length, the feeding network architecture of the switchable phased array is not illustrated in the paper. The feeding network architecture is similar to the one shown in the Fig. 3 of [7]. The 8 cables of each subarray will be connected to a digital beamforming chip or a hybrid analog/digital feeding network. Three excitations are required for three subarrays. Furthermore, if a switch is added to switch among three subarrays, only one excitation is needed for the whole array. In order to avoid the interference of the cables and the feeding network to the slot antenna array, a three-layer chassis can be applied. The top and bottom layers are copper with slot antennas on both layers. Metallized vias can be added around the edge of each slot antenna element, where the vias connect the top and bottom copper layers. Between the two copper layers are a dielectric substrate inside which micro-coaxial feeding cable and feeding networks can be integrated [26]. In this way, a reduction of the excitation can be realized with a still large coverage efficiency.

IV. Experiments and Discussions

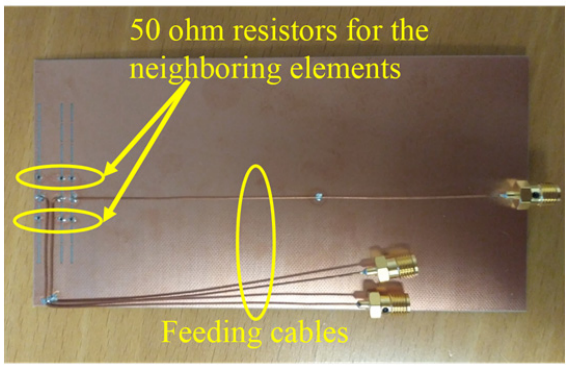

Fig. 11. Prototype of the proposed antenna. (Unit: mm)

In order to verify the performance of the proposed switchable array, a prototype has been fabricated and illustrated in Fig. 11, where the compact array structure can be observed clearly. In the measurements, element 4, element 12 and element 20 (see Fig. 2) are fed with 50 ohm thin cables. The neighboring elements of the fed elements are terminated with 50-ohm resistors, while the rest elements are kept open. The mutual coupling between the fed elements and the open elements is always lower than -20 dB. From our studies, whether terminating the open elements with 50-ohm loads or not has very limited effects on the performance of the element 4, element 12 and element 20.

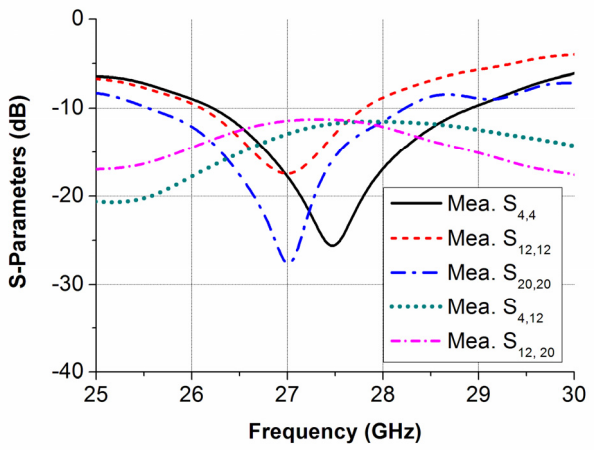

Fig. 12. Measured S-parameters with feeding cables for the element 4 in subarray A, element 12 in subarray B and element 20 in subarray C (see Fig. 2).

The S-parameters of the switchable array elements are measured. The measured S-parameters of element 4, element 12 and element 20 (see Fig. 2) are shown in Fig. 12. During all the measurements in this paper, when one element is under test (or excited), all the other elements are terminated with 50-ohm loads. In general, the measured S-parameters agree well with the simulations. It is also noticed that the operating frequencies of antenna elements in the measurements have been slightly tuned to the lower frequencies. It is mainly caused by the

This article has been accepted for publication in a future issue of this journal, but has not been fully edited. Content may change prior to final publication. Citation information: DOI 10.1109/TAP.2017.2681463, IEEE Transactions on Antennas and Propagation

manual cable soldering, where the soldered feeding points may not be exactly at the same location as those in the simulations.

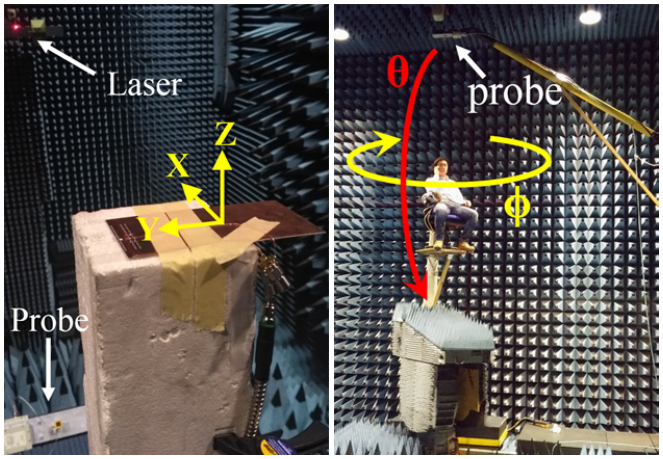

(a) (b)

Fig. 13. Measurement setups for: (a) free space, and (b) talk mode with a real person.

The gain patterns of the switchable array elements in free space and in talk mode are measured in an anechoic chamber at Aalborg University. The measurement setups are as shown in Fig. 13. A positioner rotates in ϕ direction of 0º- 360º, while a scan arm scans in θ direction of 0º- 140º. A probe horn antenna with two ports for two orthogonal polarizations is attached at the end of the scan arm. The gain of each polarization in the measurement system is calibrated with a standard gain horn antenna. At 28 GHz, the standard horn antenna has the gain of 18.52 dBi, and the 3 dB beamwidth of smaller than 22º in both E plane and H plane. The gain calibrations are carried out both before the free space measurement and before the talk mode measurement. A laser system is also installed in the chamber in order to facilitate finding the center of the measurement system. In all the measurements, the antenna under test is adjusted with the laser to be in the center of the measurement system.

The coordinate system of the measurement in free space is given in Fig. 13 (a). Since the scan arm can only scan from 0º to 140º in the θ direction, the gain pattern of each antenna in the +z axis half sphere is measured first, and then the antenna is turned over to measure the pattern in the -z axis half sphere. The comparison between the measured and simulated gain patterns of element 4, element 12 and element 20 at 28 GHz are shown Fig. 14. The beam switching property can be observed clearly in both simulations and measurements, where good alignments are obtained. In addition, the surface waves of element 4 and element 12 in –y axis direction (see Fig. 13 (a)) are slightly higher in the measurements than the simulations. It might be caused by the slightly higher substrate dielectric permittivity in the experiment than that in the simulation. The higher substrate dielectric permittivity enhances the surface waves.

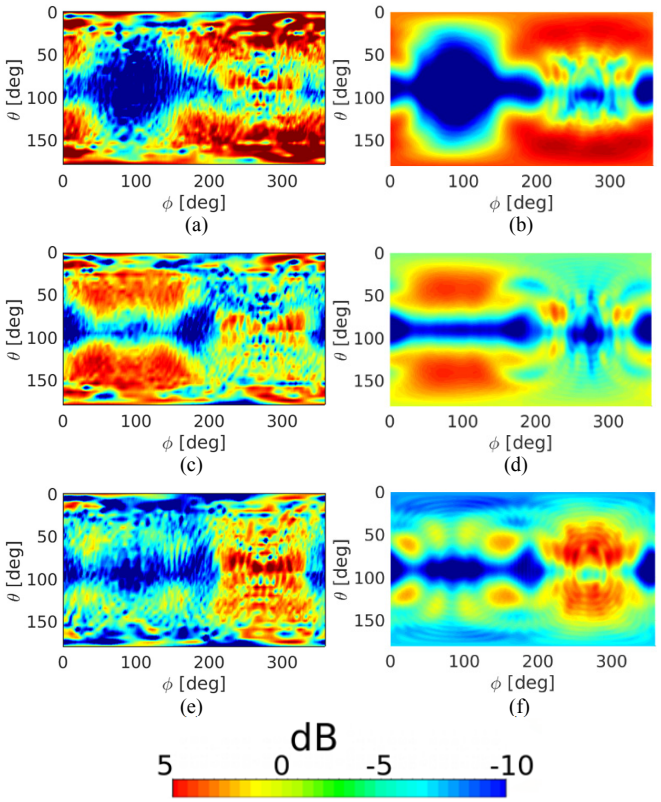

Fig. 14. Measured gain patterns at 28 GHz of (a) element 4, (c) element 12, and (e) element 20; simulated gain patterns at 28 GHz of (b) element 4, (d) element 12, and (f) element 20. (θ: 0º- 180º, ϕ: 0º- 360º)

Since commercial CTIA phantoms at 28 GHz are still not available in the market, the measurements are carried out with a real human, as shown in Fig. 13 (b). It is very challenging to keep the real human's gesture and geometry exactly the same as those of the simulated CTIA phantoms. To minimize the errors introduced by the differences from the gesture and the geometry, the switchable array at the top in talk mode is chosen for measurements to verify the simulations. The comparison between the measured and simulated results of element 4, element 12 and element 20 in the user case at 28 GHz are provided in Fig. 15. To facilitate the comparison, the simulations in Fig. 15 are obtained by replotting the results in Fig. 8 with the same ranges (of the color bar, and the θ angles) as the measurement in Fig. 15. It is seen that the gain patterns of element 4 and element 12 are similar in the simulations and measurements. The beams of element 20 point to the user's cheek and hand. As illustrated in Fig. 15 (e) and Fig. 15 (f), the beam of element 20 in the simulation is more severely reflected by tissues compared with the measurement. This may be because the angle between the phone chassis and the cheek is a little larger in the measurement with a real human than that in the simulation with CTIA phantoms. This angle difference is difficult to control. In general, the measurements still align well with the simulations.

This article has been accepted for publication in a future issue of this journal, but has not been fully edited. Content may change prior to final publication. Citation information: DOI 10.1109/TAP.2017.2681463, IEEE Transactions on Antennas and Propagation

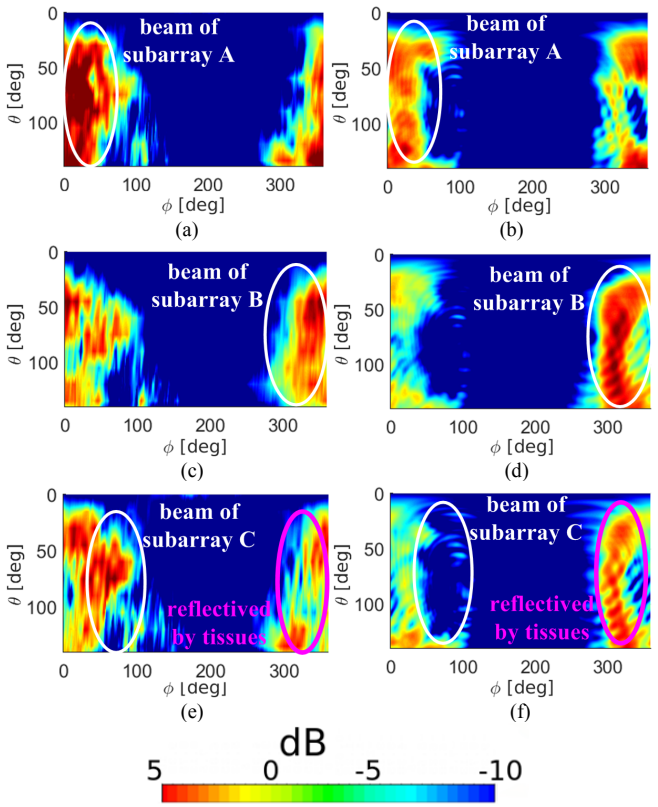

Fig. 15. Measured gain patterns in talk mode with a real person at 28 GHz of (a) element 4, (c) element 12, and (e) element 20; simulated gain patterns in talk mode with CTIA phantoms at 28 GHz of (b) element 4, (d) element 12, and (f) element 20. (θ: 0º- 140º, ϕ: 0º- 360º)

V. Conclusions

A planar switchable 3D-coverage phased array antenna has been proposed for 5G mobile terminals. 3D-coverage beam scan has been realized with a simple planar array by efficiently exciting and controlling chassis surface waves. Three identical slot subarrays have been applied to form three switchable beams to distinct regions, and within each region, there is one subarray operating as a phased array for beam steering. The bandwidth of over 2 GHz has been achieved in the 28 GHz band with large coverage efficiency. The user effects on the proposed switchable 3D-coverage phased array have been studied for data mode and talk mode (voice) at 28 GHz. It is concluded that the switchable array with three subarrays should be allocated on the top of the terminal, which always gives better beam switching, less body loss and higher realized gain than the placement at the bottom in both talk mode and date mode. An additional linear array added at the bottom for "diversity" to reduce the shadowing in talk mode. The designed antenna has been fabricated. S-parameters and gain patterns have been measured and compared with the simulations. The measured results have agreed well with the simulations.

References

[1] Z. Pi and F. Khan, "An introduction to millimeter-wave mobile broadband systems," *IEEE Commun. Mag.*, vol. 49, no. 6, pp. 101–107, 2011.

[2] T. S. Rappaport, S. Sun, R. Mayzus, H. Zhao, Y. Azar, K. Wang, G. N. Wong, J. K. Schulz, M. Samimi, and F. Gutierrez, "Millimeter wave mobile communications for 5G cellular: It will work!," *IEEE Access*, vol. 1, pp. 335–349, 2013.

[3] T. Bai, and R. Heath. "Coverage and rate analysis for millimeter wave cellular networks", *IEEE Trans. Wireless Commun.*, vol.14, no. 2, pp. 110-1114, 2015.

[4] A. Alejos, M. G. Sanchez, I. Cuinas, "Measurement and analysis of propagation mechanisms at 40 GHz: Viability of site shielding forced by obstacles," *IEEE Trans. Veh. Technol.*, vol. 57, no. 6, pp. 3369–3380, 2008.

[5] A. Balanis, *Antenna Theory*, 2nd edition, John Wiley & Sons, USA, 1997.

[6] M. Ettorre, R. Sauleau, and L. L. Coq, "Multi-beam multi-layer leaky-wave SIW pillbox antenna for millimeter-wave applications," *IEEE Trans. Antennas Propag.*, vol. 59, no. 4, pp. 1093-1100, 2011.

[7] Y. J. Cheng, H. Xu, D Ma, J. Wu, L. Wang, and Y. Fan, "Millimeter-wave shaped-beam substrate integrated conformal array antenna" *IEEE Trans. Antennas Propag.*, vol. 61, no. 9, pp. 4558-4566, 2013.

[8] J. Helander, K. Zhao, Z. Ying, and D. Sjoberg, "Performance analysis of millimeter wave phased array antennas in cellular handsets," *IEEE Antenna Wireless Propag. Lett.*, vol. 15, 2016.

[9] I. Syrytin, S. Zhang, and G. F. Pedersen, "Performance investigation of a mobile terminal phased array with user effects at 3.5 GHz for LTE advanced," *IEEE Antennas wireless Propag. Lett.,* 2016. (in press)

[10] W. Hong, K. Baek, Y. Lee, and Y. G. Kim, "Design and analysis of a low-profile 28 GHz beam steering antenna solution for future 5G cellular applications," *IEEE Int. Microw. Symp.*, Tampa Bay, Florida, 2014.

[11] N. Ojaroudiparchin, M. Shen, S. Zhang, and G. F. Pedersen, "A switchable 3D-coverage phased array antenna package for 5G mobile terminals," *IEEE Antennas Wireless Propag. Lett.,* 2016. (in press)

[12] B. Xu, K. Zhao, Z. Ying, S. He and J. Hu, "Investigation of surface waves suppression on 5G handset devices at 15 GHz," *the 10th European Conf. Antennas Propag. (EuCAP)*, 10-15 Apr., 2016.

[13] M. Pelosi, O. Franek, M. B. Knudsen, G. F. Pedersen, and J. B. Andersen, "Antenna proximity effects for talk and data modes in mobile phones," *IEEE Antennas Propag. Mag.*, vol. 52, no. 3, pp. 15–26, Jun. 2010.

[14] J. IIvonen, O. Kivekas, J. Holopainen, R. Valkonen, K. Rasilainen, and P. Vainikainen, "Mobile terminal antenna performance with the user's hand: Effect of antenna dimensioning and location," *IEEE Antennas Wireless Propag. Lett.,* vol. 10, pp. 772–775, 2011.

[15] S. Zhang, K. Zhao, Z. Ying, and S. He, "Adaptive quad-element multi-wideband antenna array for user-effective LTE MIMO mobile terminals," *IEEE Trans. Antennas Propag.*, vol. 6, no. 8, pp. 4275–4283, Aug. 2013.

[16] I. Syrytsin, S. Zhang, G. Pedersen, K. Zhao, T. Bolin and Z. Ying, "Statistical investigation of the user effects on mobile terminal antennas for 5G applications," *IEEE Trans. on Antennas Propag.*, in press.

[17] E. Safin, and D. Manteuffel, "Manipulation of Characteristic Wave Modes by Impedance Loading," *IEEE Trans. Antennas Propag.*, vol.63, no.4, pp.1756-1764, April 2015.

[18] S. Zhang, K. Zhao, Z. Ying, and S. He, "Investigation of diagonal antenna-chassis mode in mobile terminal LTE MIMO antennas for bandwidth enhancement," *IEEE Antennas Propag. Mag.*, vol. 57, no. 2, pp. 217-228, Aug. 2015.

[19] Z. Miers and B. K. Lau, "Wideband characteristic mode tracking utilizing far-field patterns," *IEEE Antennas Propag. Lett.* , vol. 14, pp. 1658–1661, Aug. 2015.

[20] D. Sievenpiper, L. Zhang, F. J. Broas, N. G. Alexopulos, E. Yablonovitch, "High-impedance electromagnetic surfaces with a forbidden frequency band", *IEEE Trans. Microwave Theory Tech.*, vol. 47, pp. 2059-2074, Nov. 1999.

[21] K. A. Norton, "The physical reality of space and surface waves in the radiation field of radio antennas," *Proceedings of the Institute of Radio Engineers*, vol. 25, no.9, pp. 1192-1202, September 1937.

[22] S. Stein, "On cross coupling in multiple-beam antennas," *IEEE Trans. Antennas Propag.*, vol. 10, no. 5, pp. 548–557, Sep. 1962.

[23] J. Wang, Z. Lan, C.-W. Pyo, et al, "Beam codebook based beamforming protocol for multi-Gbps millimeter-wave WPAN systems," *IEEE J. Select. Areas Commun.*, vol. 27, no. 8, pp. 1390-1399, Oct. 2009.

[24] C. Gabriel, S. Gabriel and E. Corthout "The dielectric properties of biological tissues: I. Literature survey" *Phys. Med. Biol.*, vol. 41, pp. 2231–2249, 1996.

[25] Test plan for Mobile Station Over the Air Performance CTIA revision 3.1, Jan. 2011.

[26] K. Vanhille, M. Lukic, S. Rondineau, D. Filipovic, Z. Popovic, "Integrated micro-coaxial passive components for millimeter-wave antenna front ends," *Proc. 4th IASTED Int. Conf. Antennas Radar Wave Propag*., 2007.